Wave-equation tomography: I

Marta Jo Woodward

ABSTRACT

Wave-theoretic, diffraction tomography is usually formulated in the spatial-frequency domain. This paper reformulates the method in the space domain, for the purpose of clarifying its relation to ray-theoretic tomography. Where ray-theoretic tomography projects traveltimes back over *raypaths*, space-domain, wave-equation tomography projects differential wavefields back over *wavepaths*. Comparison of raypaths and wavepaths reveals the different assumptions the two methods make about the seismic experiment: specifically, about amplitudes, frequency dispersion and event discrimination. Through examination of these assumptions, wavepaths are identified as monochromatic raypaths, and bandlimited raypaths are defined as wavepaths averaged over frequency. Examples of ray-theoretic and wave-equation tomographic inversions are shown for a finite-difference data set.

INTRODUCTION

Seismic tomography iteratively reconstructs a velocity field from integrals through the field. When the field varies slowly on the scale of the source wavelengths, phase velocity and group velocity are equivalent; the medium is nondispersive and ray-theoretic, traveltime tomography may be applied. For each event and each source-receiver pair, a single traveltime delay is picked and backprojected over the corresponding raypath. When the field varies rapidly on the scale of the source wavelengths, phase velocity and group velocity are not equivalent; the medium is dispersive and wave-theoretic, diffraction tomography must be applied. The scattered wavefield is backpropagated using the scalar wave equation, after linearization through application of either the Born or Rytov approximation.

Diffraction tomography has usually been presented in the Fourier domain, for single frequency sources (Devaney, 1982; Slaney, 1984; Wu and Toksoz, 1987). This paper formulates diffraction tomography as a multifrequency backprojection problem in the space domain. Just as traveltime delays are projected back over source-receiver *raypaths* in ray-theoretic tomography, scattered amplitudes and phases may be projected back over source-receiver *wavepaths* in wave-equation tomography. The wavepaths are described by elliptical, multiple-Fresnel-zone patterns, calculated for each source frequency to accommodate dispersion.

This paper is organized into six main sections. The first four discuss the theory of wave-equation tomography: they derive ray-theoretic and wave-equation tomography in a parallel fashion, then compare their respective raypaths and wavepaths. The fifth section introduces a cross-hole geometry, finite-difference data set, and examines wave-equation tomography as a forward-modelling method similar to raytracing. The sixth section addresses the sampling problem in space-domain, wave-equation tomography, and shows inversions of several subsets of the data set. This paper is meant to complement another in this volume (Rocca and Woodward, 1988), which presents many of the same ideas from a different viewpoint.

TOMOGRAPHIC EQUATIONS

Ray-theoretic tomography

Seismic tomography reconstructs a velocity field from integrals through the field (Fawcett and Clayton, 1984). In ray-theoretic applications, the integrals are traveltimes measured for shot-geophone pairs $(\mathbf{s},\mathbf{g})$. They correspond to integrations along raypaths through the velocity field expressed as slowness (w):

$$t(\mathbf{g}|\mathbf{s}) = \int w(\mathbf{r}) L(\mathbf{r}|\mathbf{s},\mathbf{g},w) d\mathbf{r}. \tag{1}$$

Because $L(\mathbf{r})$—the raypath—is a function of w, the problem is nonlinear. The equation is generally linearized in two steps. First, the slowness field is decomposed into a background field plus a perturbed field:

$$t_0(\mathbf{g}|\mathbf{s}) = \int w_0(\mathbf{r}) L_0(\mathbf{r}|\mathbf{s},\mathbf{g},w_0) d\mathbf{r} \tag{2}$$

$$\Delta t(\mathbf{g}|\mathbf{s}) = \int \Delta w(\mathbf{r}) L(\mathbf{r}|\mathbf{s},\mathbf{g},w) d\mathbf{r}. \tag{3}$$

Second, using Fermat's principle, the raypath is approximated by the raypath through the background field:

$$\Delta t(\mathbf{g}|\mathbf{s}) = \int \Delta w(\mathbf{r}) L_0(\mathbf{r}|\mathbf{s},\mathbf{g},w_0) d\mathbf{r}. \tag{4}$$

Consideration of a number of shots and geophones generates a system of equations—$L\Delta w = \Delta t$—that can be solved by any of a number of matrix methods. The nonlinear part of the problem is attacked iteratively, by forward modelling (raytracing) through the updated field after each linear step.

Wave-equation tomography

Wave-theoretic tomography may be formulated in an analogous fashion. The equations are developed here in two ways: the first leading to a linearization of the scalar wave equation with the Born approximation; the second leading to a linearization with the Rytov approximation.

For the Born approximation, the differential traveltimes of ray-theoretic tomography are replaced by complex numbers. These are differential, frequency-domain wavefields—$\Delta\psi(\omega)$—measured for shot-geophone pairs. The monochromatic analog of Equation 3 is:

$$\Delta\psi(\mathbf{g}|\mathbf{s}) = \int O(\mathbf{r})G(\mathbf{g}-\mathbf{r})\psi(\mathbf{r}|\mathbf{s},O)d\mathbf{r}, \tag{5}$$

(Slaney, op. cit.). Here G is the free-space Green's function: for 3-dimensions,

$$G(\mathbf{r}) = \frac{e^{ik_0|\mathbf{r}|}}{4\pi|\mathbf{r}|}; \tag{6}$$

for 2-dimensions,

$$G(\mathbf{r}) = \frac{i}{4}H_0^{(1)}(k_0|\mathbf{r}|). \tag{7}$$

($H_0^{(1)}$ is a zero-order Hankel function of the first kind and $k_0 = \omega/v_0$.) $O(\mathbf{r})$ is known in the literature as the object function, the differential velocity field expressed as

$$O(\mathbf{r}) = 2k_0^2\frac{\Delta v}{v}. \tag{8}$$

Interpreted physically, Equation 5 says the anomalous wavefield at a specific geophone is generated by superposition: each point in the medium acts as a scatterer, with a magnitude equal to the product of the full wavefield and the object function at that point. Interpreted algorithmically and rewritten as:

$$\Delta\psi(\mathbf{g}|\mathbf{s}) = \int \frac{\Delta v(\mathbf{r})}{v(\mathbf{r})}\mathcal{L}(\mathbf{r}|\mathbf{s},\mathbf{g},v)d\mathbf{r}, \tag{9}$$

the equation says the differential wavefield is an integration through the differential velocity field over the monochromatic *wavepath* $\mathcal{L}$. As in the ray-theoretic application, $\mathcal{L}$ (specifically, ψ) is a function of O, and the problem is nonlinear. Under the Born approximation, the equation is linearized by assuming the wavepath $\mathcal{L}$ to be independent of the differential velocity field, yielding the analog of Equation 4:

$$\Delta\psi(\mathbf{g}|\mathbf{s}) = \int \frac{\Delta v(\mathbf{r})}{v(\mathbf{r})}\mathcal{L}_0(\mathbf{r}|\mathbf{s},\mathbf{g},v_0)d\mathbf{r}. \tag{10}$$

For a point source at $\mathbf{s}$, ψ_0 is the free-space Green's function, and

$$\mathcal{L}_0(\mathbf{r}|\mathbf{s}) = 2k_0^2G(\mathbf{g}-\mathbf{r})G(\mathbf{s}-\mathbf{r}). \tag{11}$$

The Born approximation applies where the magnitude of the differential field ($\Delta\psi$) is smaller than that of the incident field (ψ_0)—implying the change in phase between the incident field and the wave propagating through the object is less than π (Slaney, op. cit.). In practical terms this restriction means the Born approximation can deal with large deviations in the velocity field, confined to small regions in space. This last requirement corresponds poorly with the assumptions of ray-theoretic tomography. Wave-equation tomography under the Born approximation and ray-theoretic tomography cannot usually be applied to the same velocity field.

For the Rytov approximation, the traveltimes of ray-theoretic tomography are replaced by the differential complex logarithm ($\Delta\phi = \ln(\psi/\psi_0)$) of the frequency domain wavefields—measured for shot-geophone pairs. The monochromatic analog of Equation 3 is:

$$\Delta\phi(\mathbf{g}|\mathbf{s}) = \int \frac{G(\mathbf{r})\psi_0(\mathbf{r}|\mathbf{s})}{\psi_0(\mathbf{g}|\mathbf{s})}((\nabla(\Delta\phi(\mathbf{r}|\mathbf{s},O))^2 + O(\mathbf{r}))d\mathbf{r}, \tag{12}$$

(Slaney, op. cit.). This equation is more difficult to interpret physically than the Born equivalent. However, under the Rytov approximation, $(\nabla(\Delta\phi))^2$ is assumed to be much smaller than O, and Equation 12 becomes

$$\Delta\phi(\mathbf{g}|\mathbf{s}) = \int O(\mathbf{r})\frac{G(\mathbf{g}-\mathbf{r})\psi_0(\mathbf{r}|\mathbf{s})}{\psi_0(\mathbf{g}|\mathbf{s})}d\mathbf{r}. \tag{13}$$

This equation may then be rewritten as:

$$\Delta\phi(\mathbf{g}|\mathbf{s}) = \int \frac{\Delta v(\mathbf{r})}{v(\mathbf{r})}\mathcal{L}_0(\mathbf{r}|\mathbf{s},\mathbf{g},v_0)d\mathbf{r} \tag{14}$$

—and the differential complex phase again viewed as an integration through the differential velocity field over a wavepath. For a point source at $\mathbf{s}$, ψ_0 is the free-space Green's function, and

$$\mathcal{L}_0(\mathbf{r}|\mathbf{s}) = 2k_0^2\frac{G(\mathbf{g}-\mathbf{r})G(\mathbf{s}-\mathbf{r})}{G(\mathbf{s}-\mathbf{g})}. \tag{15}$$

The Rytov approximation holds where the change in the logarithm of the scattered wavefield over one wavelength is small (Slaney, op. cit.). While the approximation works best in applications where velocity variations are small in magnitude, no limitations are placed on the spatial extent of the anomalous velocity field. The Rytov approximation is more likely than the Born approximation to apply where the assumptions of ray-theoretic tomography are met.

Whereas ray-theoretic tomography forms a system of equations through consideration of a number of shots and geophones, wave-equation tomography forms a system of equations—$\mathcal{L}\Delta v/v = \Delta\psi$ or $\mathcal{L}\Delta v/v = \Delta\phi$—through consideration of a number of shots, geophones and frequencies. As before, the nonlinear part of the problem is attacked iteratively, by wave-equation modelling through the updated

field after each linear step. The fifth and sixth sections of this paper show examples of wave-equation tomography applied to forward modelling and inversion.

WAVEPATHS

Born and Rytov approximation examples of $\mathcal{L}$ for monochromatic, 5 and 10 Hz sources in a cross-hole geometry are shown in Figures 1a through 1d. The applicable background velocity field is a constant 2000 m/s; the sources and geophones are separated by 2000 m, and the source wavefields are 2-dimensional Green's functions. Note that each wavepath has a real and an imaginary part. While the complex absolute values of the wavepaths decay as $1/\sqrt{(\mathbf{g}-\mathbf{r})(\mathbf{s}-\mathbf{r})}$, the phase of the patterns oscillates from π to $-\pi$. Contours of the real and imaginary wavepaths yield concentric ellipses, with sources and geophones located at the foci.

In the Rytov wavepath, phase and amplitude separate naturally—just as time delay and amplitude separate in ray-theoretic tomography. When multiplied by the object function, the imaginary part of the Rytov wavepath yields the phase delay between $\psi(\omega)$ and $\psi_0(\omega)$; the real part of the wavepath yields the log of the amplitude ratio, $\ln(|\psi(\omega)|/|\psi_0(\omega)|)$. The imaginary part of the pattern passes through zeroes at the boundaries between the first, second, third, etc. Fresnel zones. A scatterer within the first Fresnel zone generates a wavefield reaching the geophone within a half wavelength of the source wavefield: a low velocity scatterer produces a phase delay; a high velocity scatterer produces a phase advance. A scatterer in the second Fresnel zone generates a wavefield reaching the geophone between a half and a full wavelength behind the source wavefield: a low velocity scatterer produces a phase advance; a high velocity scatterer produces a phase delay. Similar arguments about amplitudes explain the ups and downs of the real part of the Rytov wavepath.

In the Born wavepath, phase and amplitude are intermixed. When multiplied by the object function, the real part of the Born wavepath yields $Re(\psi(\omega)-\psi(\omega))$; the imaginary part of the wavepath yields $Im(\psi(\omega)-\psi(\omega))$. Neither of these quantities have analogs in ray-theoretic tomography. The quantities do have analogs in migration theory, and the ellipses in the Born wavepaths are closely related to migration ellipses.

WAVEPATHS VS. RAYPATHS: SPACE DOMAIN

Figure 1e shows a raypath, the ray-theoretic equivalent of the Rytov wavepaths in Figures 1a and 1c. Three major differences between the raypath and the wavepaths should be noted. First, while integration through a velocity field along a raypath yields one measurement—a traveltime—integration along a wavepath yields two measurements—one real and one imaginary. Second, while ray-theoretic tomography projects information back over one raypath for each shot-geophone pair,

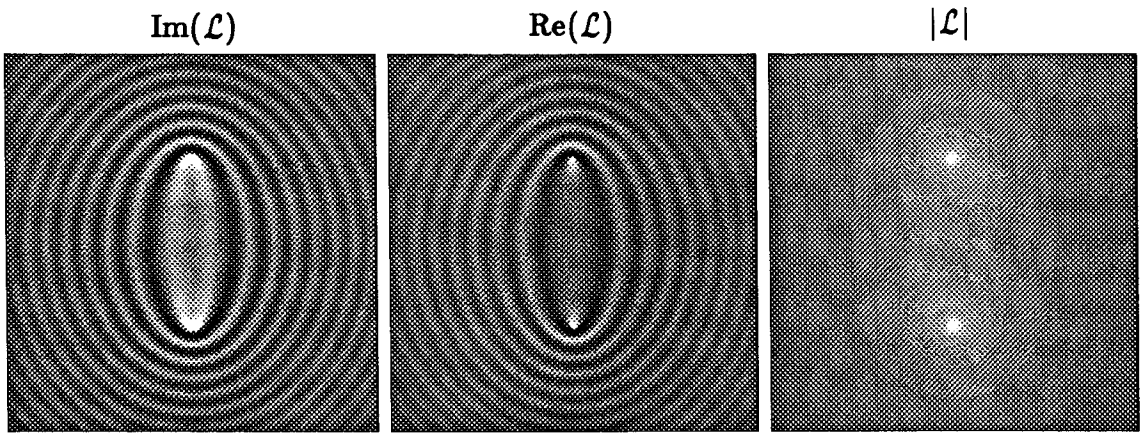

a) 5 Hz wavepath: Rytov approximation

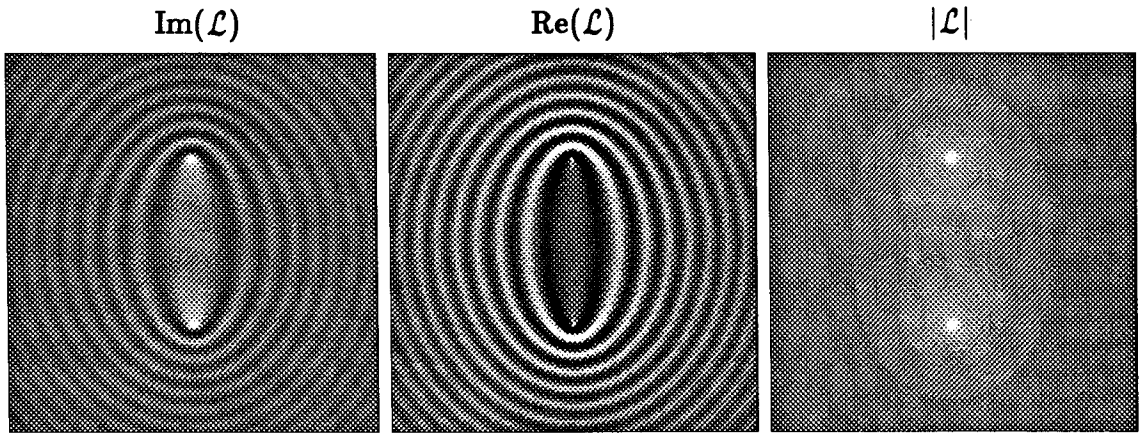

b) 5 Hz wavepath: Born approximation

FIG. 1. (a), (b) Rytov and Born approximation wavepaths $\mathcal{L}$ for a 5 Hz source, respectively. Parts (c), (d), and (e) are on the facing page.

wave-equation tomography projects information back over one wavepath for each frequency considered. Third, while a raypath interrogates a small region of the velocity field, a wavepath interrogates the whole field. Analysis of these differences reveals the contrasting assumptions ray-theoretic and wave-theoretic tomography make about the availability of information in the seismic experiment. The following three subsections examine the implications of these differences.

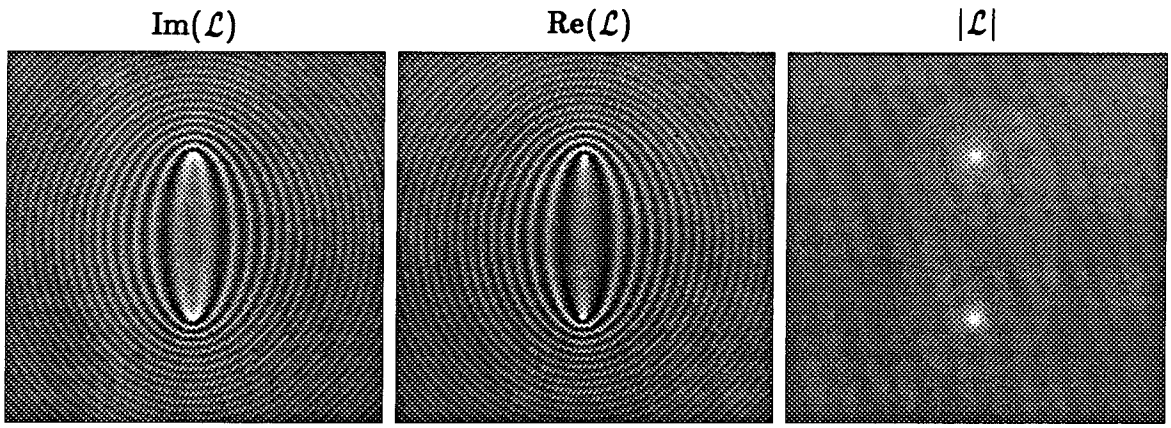

c) 10 Hz wavepath: Rytov approximation

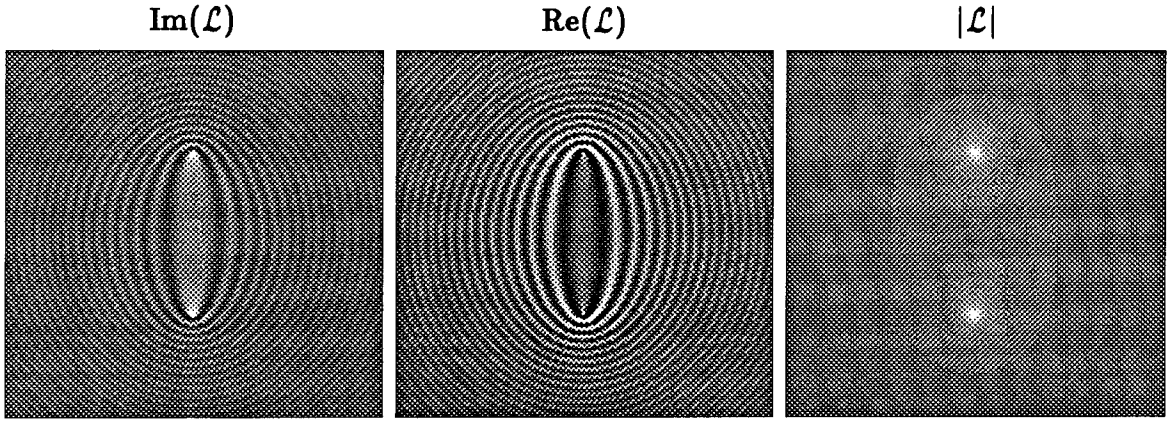

d) 10 Hz wavepath: Born approximation

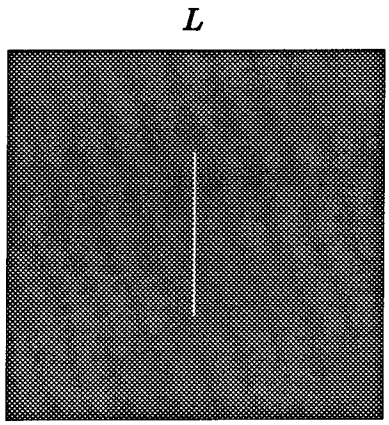

e) raypath

FIG. 1. (c), (d) Rytov and Born approximation wavepaths $\mathcal{L}$ for a 10 Hz source; (e) the raypath L equivalent of $\mathcal{L}$.

Amplitudes

The first difference underlines the fact that, by ignoring amplitudes, ray-theoretic tomography discards half of the information in the seismic experiment. It also emphasizes that ray-theoretic tomography must be compared to wave-equation tomography under the Rytov approximation, and not under the Born approximation. Amplitude and phase separate in the Rytov formulation of diffraction tomography. The differential traveltimes of ray-theoretic tomography correspond directly with the differential phases measured by the imaginary Rytov wavepaths. The fact that ray theory corresponds more closely to wave-equation tomography under the Rytov assumption than under the Born assumption is not surprising, upon recollection of the types of velocity fields to which each applies.

Frequency dispersion

Ray-theoretic tomography is usually described as applying under the high frequency assumption—where the spatial wavelengths of the seismic source are much smaller than the characteristic dimensions of the velocity field (Bleistein, 1984). With a bandlimited source, an alternative expression of the high frequency assumption might be that the velocity field is nondispersive: i.e., that all the frequencies in the seismic wavelet undergo phase shifts corresponding to a single time shift—that phase velocity and group velocity are equivalent.

Wave-equation tomography backpropagates scattered wavefields using the scalar wave equation. Consequently, perturbations to the wavefield are allowed to affect separate frequencies differently. Phase velocity and group velocity need not be equivalent; the medium can be dispersive.

This contrast between wave-equation tomography and ray-theoeretic tomography explains the second difference between the wavepaths and raypath of Figure 1: ray-theoretic tomography projects information back over one raypath for each shot-geophone pair; wave-equation tomography projects information back over one wavepath for each frequency considered. Ray-theoretic tomography lumps the single frequency experiments of wave-equation tomography into one equation.

This contrast also suggests a redefinition of ray-theoretic tomography as a subset of wave-equation tomography. The method may be viewed as wave-equation tomography under the Rytov approximation—with the addition of a nondispersive constraint. A nondispersive medium implies the phase shifts experienced by each frequency (normalized by frequency) are equivalent. This assumption means that the imaginary parts of the Rytov wavepaths (normalized by frequency) may be summed over all frequencies without loss of information. Clearly, summing the imaginary wavepaths of Figure 1 over frequency yields narrow *wavepaths* resembling fat, elliptical *raypaths*: the rapidly oscillating, outer regions cancel; the smooth, innermost regions corresponding to the first Fresnel zones add. Figure 2a shows one

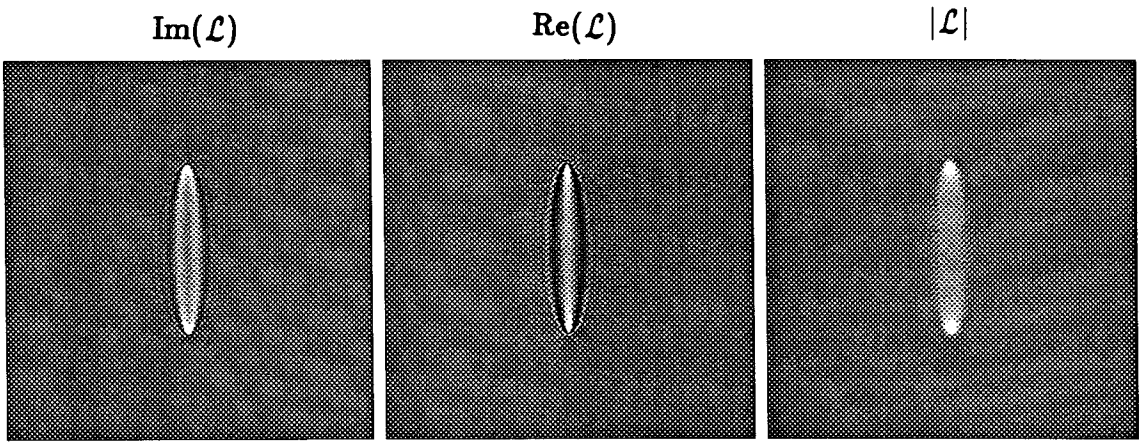

FIG. 2. Bandlimited (fat) raypath formed by integrating monochromatic wavepaths from 5 to 30 Hz. Artifacts resulting from the summation sampling interval have been removed.

of these fat raypaths, formed by integrating Rytov imaginary patterns from 5 to 30 Hz, with spatial dimensions analogous to those in Figure 1.

If nondispersive (frequency invariant) amplitude information is added into this definition of the ray, the real part of the fat raypath appears as in Figure 2b. Figure 2c shows the complex absolute value of the bandlimited raypath. The accompanying paper (Rocca and Woodward, 1988) proves the width of the bandlimited raypath depends on the width of the frequency band summed over, not on the central frequency of the band. The bandlimited raypath collapses to the familiar picture of Figure 1e for infinite bandwidth.

Substitution of a fat raypath for a traditional raypath adds a priori information to a ray-theoretic inversion, effectively reducing the null space of the problem (Woodward, 1986; Woodward, 1987). Of course, as with ray-theoretic tomography, it may accurately be used only where no dispersion is observed.

Event discrimination

The preceding subsection explained the third difference between wavepaths and raypaths as a side-effect of the second, ascribing their dissimilar spatial extents to ray-theoretic tomography's dual assumption of infinite bandwidth and nondispersion. This section reexamines the problem from another viewpoint: the difference is attributed to the contrasting ways in which ray-theoretic and wave-theoretic tomography discriminate events in the time domain.

In real data, events usually overlap. If the events result from perturbations to the same background velocity field, the overlap poses no difficulty—the events are essentially one event. If the events require linearization of the problem around different velocity fields, they must be distinguished—and separated by windowing.

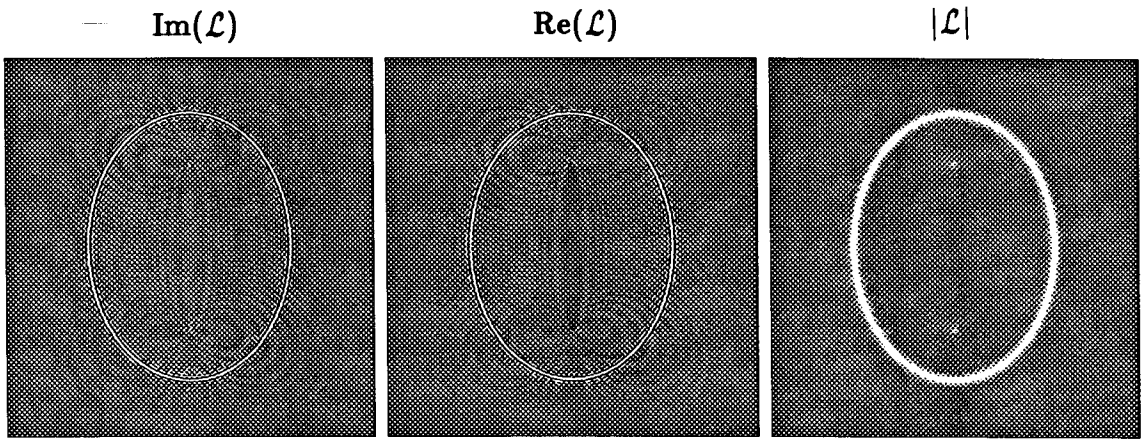

FIG. 3. Bandlimited raypath formed by integrating monochromatic wavepaths from 5 to 30 Hz, after modulation by $e^{i\omega\Delta t}$, $\Delta t = .41$ seconds. Artifacts resulting from the summation sampling interval have been removed.

Windowing an event in the time domain smooths the event in the frequency domain. This smoothing corresponds to averaging wavepaths in the space-domain over frequency. Ray-theoretic tomography assumes a window length of one time sample. For a single-sample window, a single, complex data point is obtained in the frequency domain—the average data point. As shown in the preceding section, averaging wavepaths from zero to Nyquist produces a fat raypath. For ray-theoretic tomography, the averaging only discards what is assumed to be redundant information, given the nondispersive constraint. For dispersive media, the averaging discards nonredundant information.

Wavenumber-domain diffraction tomography, as usually implemented, requires a time window of infinite length and wavepaths of infinite extent. Space-domain, wave-equation tomography is more flexible: time windows may be acknowledged by averaging monochromatic wavepaths over frequency as necessary. The narrower the window: the more global the average; the less information available; the narrower the wavepath. The broader the window: the more local the average; the more information available; the broader the wavepath.

These shrinking and expanding wavepaths have an intuitive, physical explanation in the space domain. Energy scattered by a point in an anomalous velocity field that is far from the shot-geophone axis reaches the geophone long after energy scattered by points along the axis. Wavepaths of infinite extent are applicable when distant scatterers are detectable—when time-domain data is of infinite length. Wavepaths of finite extent are applicable when distant scatterers are ignored—when time-domain data is windowed around an average (group) arrival time.

This analysis also suggests a third example: windowing time-domain data around a low energy portion of an event, trailing the group arrival by Δt. Figure 3 shows the result of summing wavepaths from 5 to 30 Hz, after multiplication by $e^{i\omega\Delta t}$.

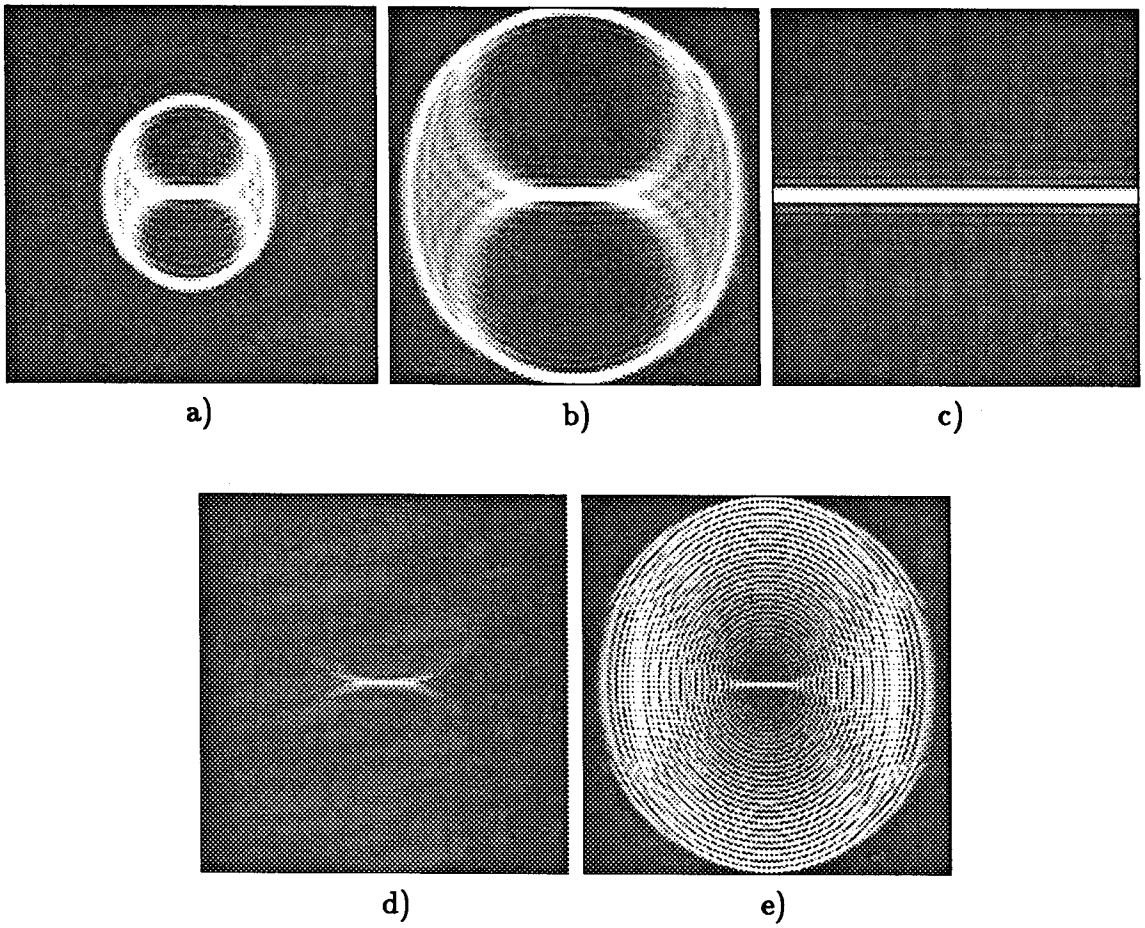

FIG. 4. Two-dimensional spatial-amplitude spectra: (a) 5 Hz wavepath; (b) 10 Hz wavepath; (c) raypath; (d) bandlimited raypath of Figure 2; (e) bandlimited, modulated raypath of Figure 3. Plots (a), (b) and (c) are shown at the same scale ($k_{max} = 2k_0$, $k_0 = 2\pi \cdot 10/v_0$), origins in the center. Plots (d) and (e) are shown at one-third the scale of (a), (b) and (c) ($k_{max} = 2k_0$, $k_0 = 2\pi \cdot 30/v_0$), origins in the center.

While the width of a time window determines the magnitude of space examined by a seismic experiment, the positioning of the time window determines the region of space examined.

WAVEPATHS VS. RAYPATHS: WAVENUMBER DOMAIN

Figures 4a, 4b, and 4c show the two-dimensional spatial-amplitude spectra of the 5 and 10 Hz wavepaths (they are the same for both the Born and Rytov patterns) and of the raypath. Both ray-theoretic and wave-theoretic tomography are most sensitive to spatial frequencies representing velocity variations paralleling the shot-geophone axis and least sensitive to those perpendicular to the axis. The wavepaths

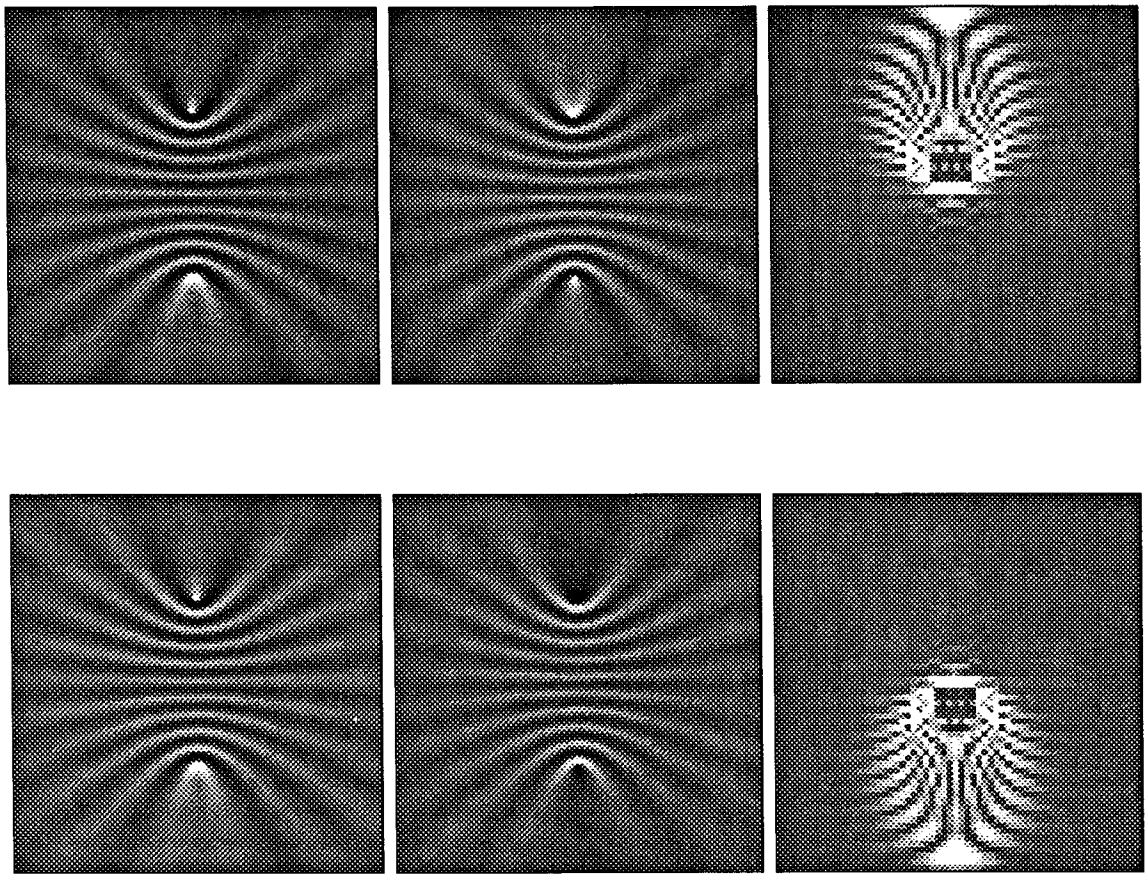

FIG. 5. Upper plot: monochromatic 5 Hz wavepath and spatial-amplitude spectrum resulting from replacement of the source Green's function in Equation 15 by $H_0^{(2)}$. Lower plot: monochromatic 5 Hz wavepath and spatial-amplitude spectrum resulting from replacement of the geophone Green's function in Equation 15 by $H_0^{(2)}$.

have a maximum spatial frequency twice that of the source wavefield, approached as a limit by the spacing of the most distant concentric ellipses. The broad coverage of the spatial-frequency domain by the transformed wavepaths results from the assumption of infinite window length in the time domain. Averaging the wavepaths in the space domain reduces their extent in the spatial frequency domain. Figures 4d and 4e show the spatial-frequency amplitude spectra of Figures 2 and 3—the finite wavepaths formed by averaging infinite wavepaths from 5 to 30 Hz.

The characteristic holes in the spatial-amplitude spectra of the monochromatic wavepaths arise from a causality (source/sink) condition placed on the source and geophone Green's functions in Equation 15. The elliptical wavepaths are formed when the Green's functions are set equal to zero-order Hankel functions of the first kind. Replacing either the source or the geophone Green's function with a zero-order Hankel function of the second kind (the complex conjugate of $H_0^{(1)}$), yields the wavepaths and spatial-amplitude spectra shown in Figure 5. The familiar ellipses

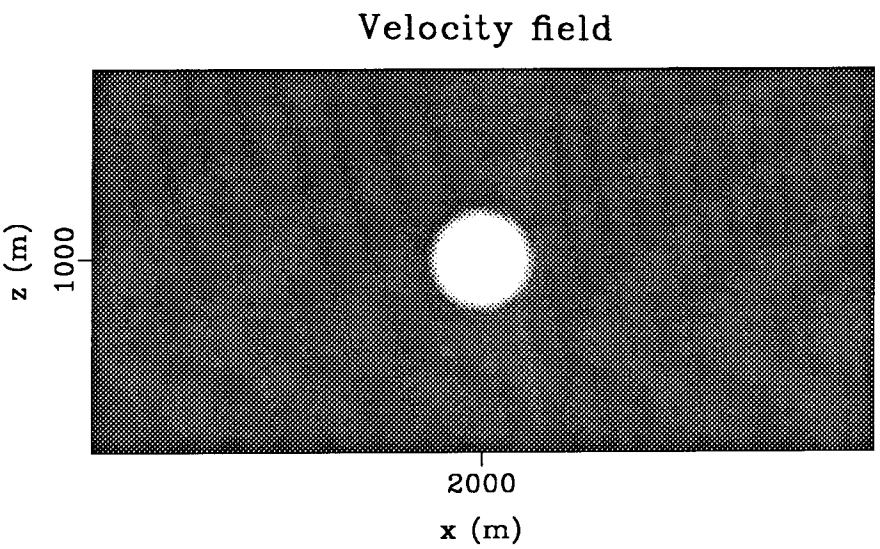

FIG. 6. Velocity field for the finite-difference modelled synthetic data set.

(the locus of points the *sum* of whose distances from source and geophone is constant) have been replaced by hyperbolae (the locus of points the *difference* of whose distances from source and geophone is constant). Physically, this transformation results from the replacement of an exploding, causal source by an imploding, anti-causal source. Just as energy from an exploding source that is scattered by points along a single ellipse reaches a geophone in phase, energy from an imploding source scattered by points along a single hyperbola reaches a geophone in phase. This point is addressed more fully in the accompanying paper (Rocca and Woodward, 1988).

NUMERICAL EXAMPLE—FORWARD MODELLING

This section provides a qualitative analysis of a finite-difference generated seismic experiment, consisting of one shot and multiple geophones in a cross-hole geometry. The purpose of the section is both to familiarize the reader with the complex data used in wave-equation tomography, and to emphasize the conceptual simplicity with which wavepaths forward model the data. The section is divided into two subsections. The first describes the experiment; the second examines the data.

The experiment

Figure 6 shows the velocity field used for the experiment: it consists of an anomalous circular region 500 m in diameter, with a velocity 5% below that of the 2000 m/s background. The shot was positioned on the surface, directly above the anomaly; the geophones were positioned at a depth of 2000 m, up to an offset of 2000 m on either side. The source wavelet was the second derivative of a Gaussian

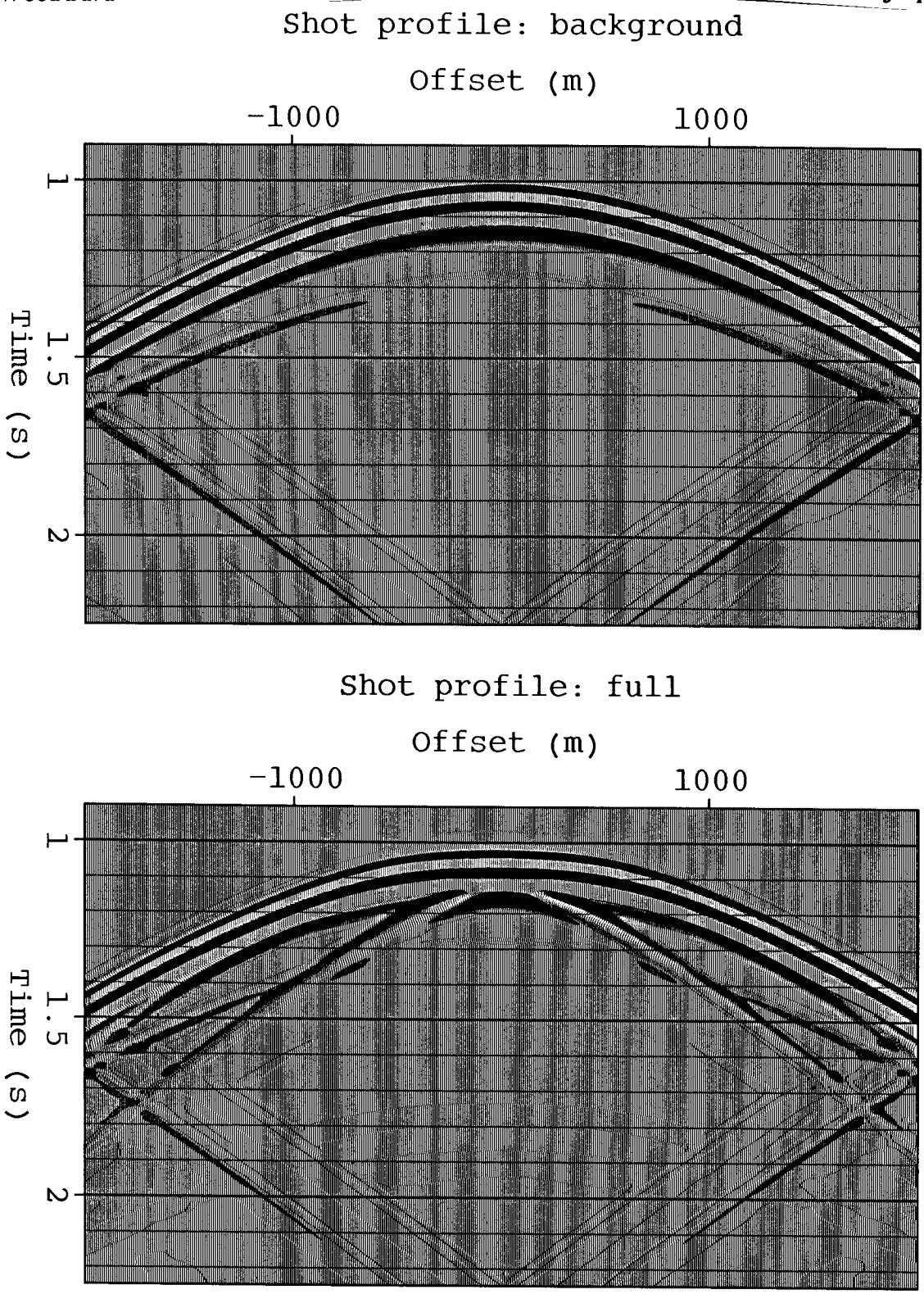

FIG. 7. (a), (b) Shot profiles generated by finite-difference modelling through the constant background and full velocity fields of Figure 6, respectively. The data was clipped to emphasize the scattered energy.

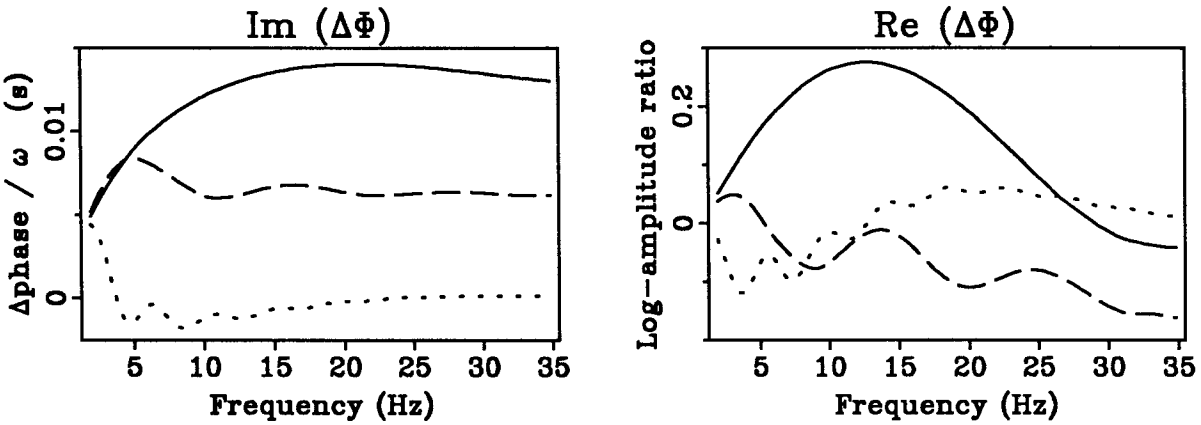

FIG. 8. The data used by Rytov wave-equation tomography. The graph on the left shows the phase delay between the perturbed and unperturbed shot profiles, plotted as a function of frequency. The phase delay has been normalized by frequency and expressed in seconds. The graph on the right shows $\ln|\psi(\omega)| - \ln|\psi(\omega)|$, plotted as a function of frequency. The solid, dashed and dotted lines indicate offsets of 0, 360 and 1060 m, respectively.

curve, bandlimited from approximately 5 to 30 Hz. Figures 7a and 7b show shot profiles generated by finite-difference modelling through the constant background field and the full field, respectively. The recording time was long enough that infinite time windows could be assumed. The circular anomaly was designed to satisfy the assumptions of the Rytov approximation.

The data

Figure 8 shows the data used by Rytov, wave-equation tomography for three traces of Figure 7 (offsets 0, 360 and 1060 m). The leftmost graph plots differential phase as a function of frequency; the rightmost graph plots log-amplitude ratio as a function of frequency. The differential phases are presented as time delays, having been normalized by frequency. In the interest of brevity, this discussion is confined to analysis of the phase plots—and consequently of the imaginary part of the Rytov wavepaths. Parallel arguments could be presented for the log-amplitude plots—and the real part of the Rytov wavepaths. Since the real and imaginary parts of the wavepaths are 90 degrees out of phase, it is not surprising that the log-amplitude plots resemble the derivatives of the phase plots.

Figures 9 and 10 are meant to illustrate the physical meaning of wavepaths as forward-modelling tools. Figure 9 overlays outlines of 5, 10, 15, 20, 25 and 30 Hz first-Fresnel zones and a contoured outline of the circular anomaly—for the three different offsets. (The reader should recall that the boundary of the first Fresnel zone is equivalent to the first zero-crossing of the imaginary Rytov wavepaths.) The absolute maxima in Figure 8 can be predicted by inspection of Figure 9: for each

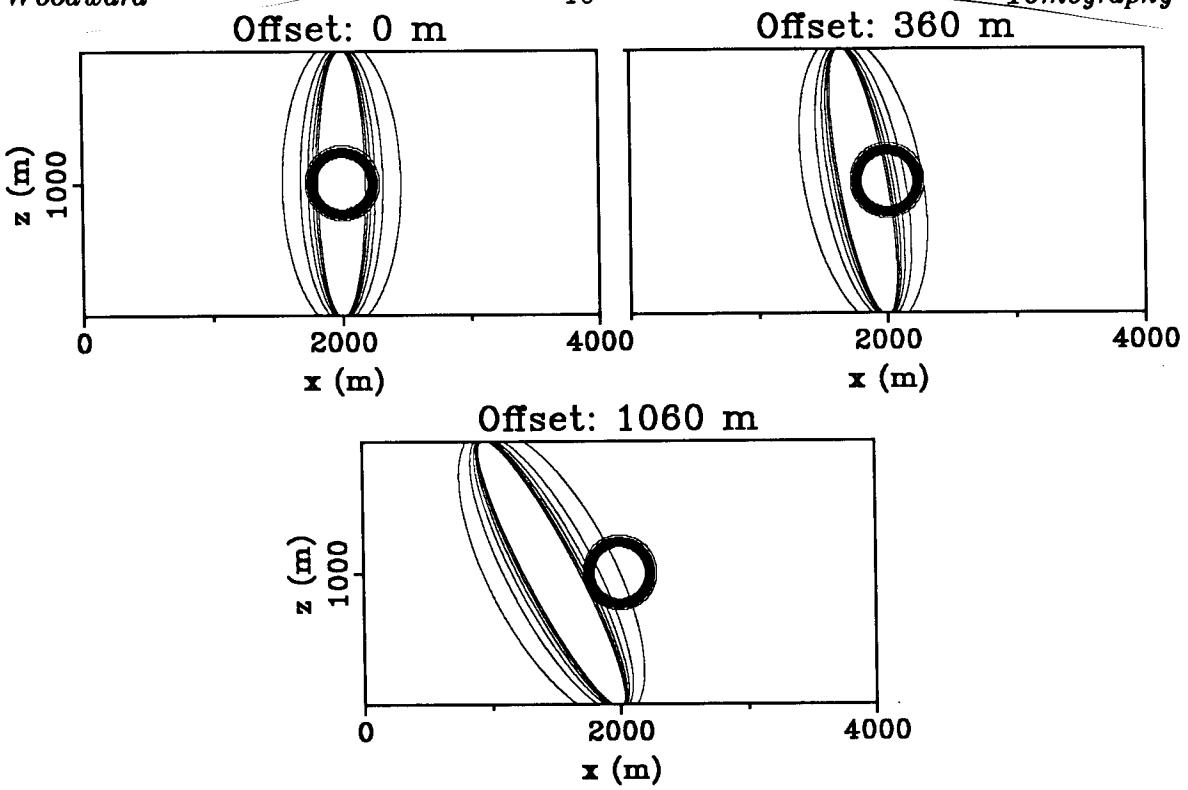

FIG. 9. First-Fresnel zones for 5, 10, 15, 20 and 25 Hz are shown superimposed on a contoured outline of the circular velocity anomaly, for offsets 0, 360 and 1060 m. The 5 Hz first-Fresnel zone is the widest.

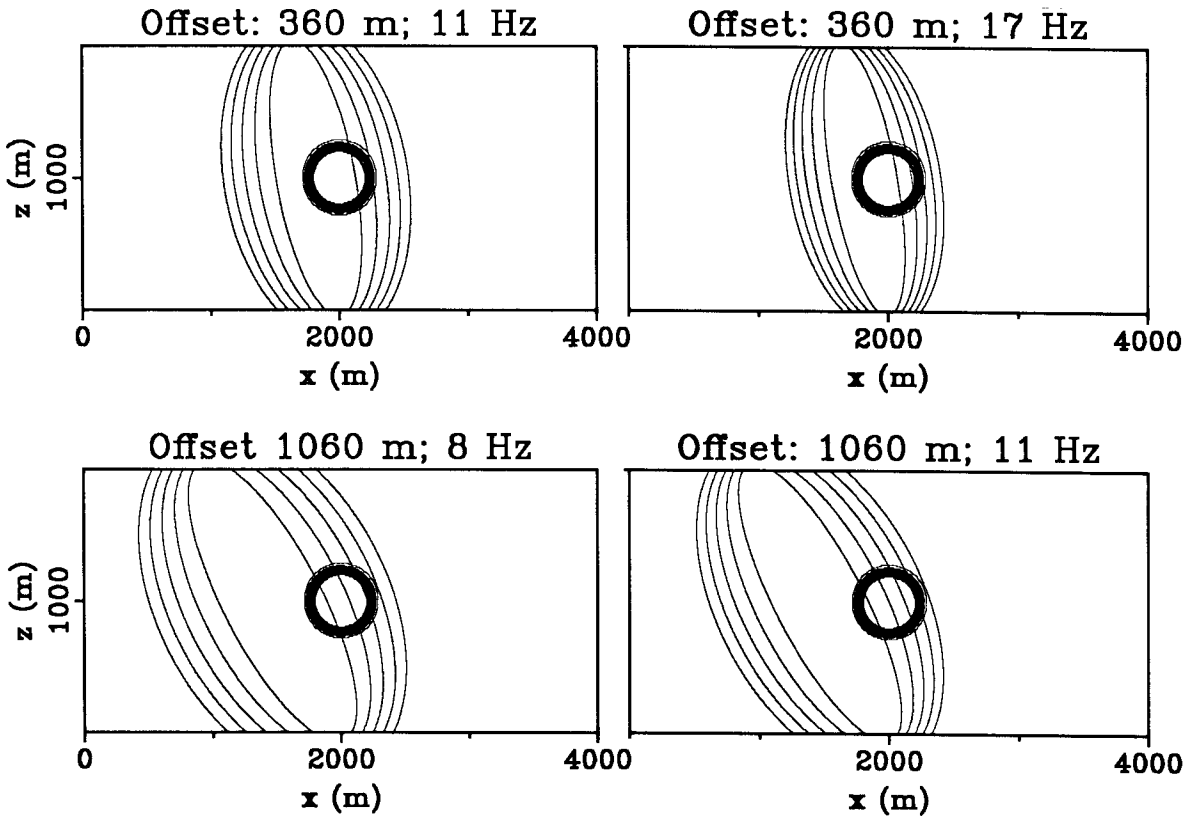

FIG. 10. The boundaries of the first five Fresnel zones for several frequencies and offsets are shown superimposed on the circular velocity anomaly.

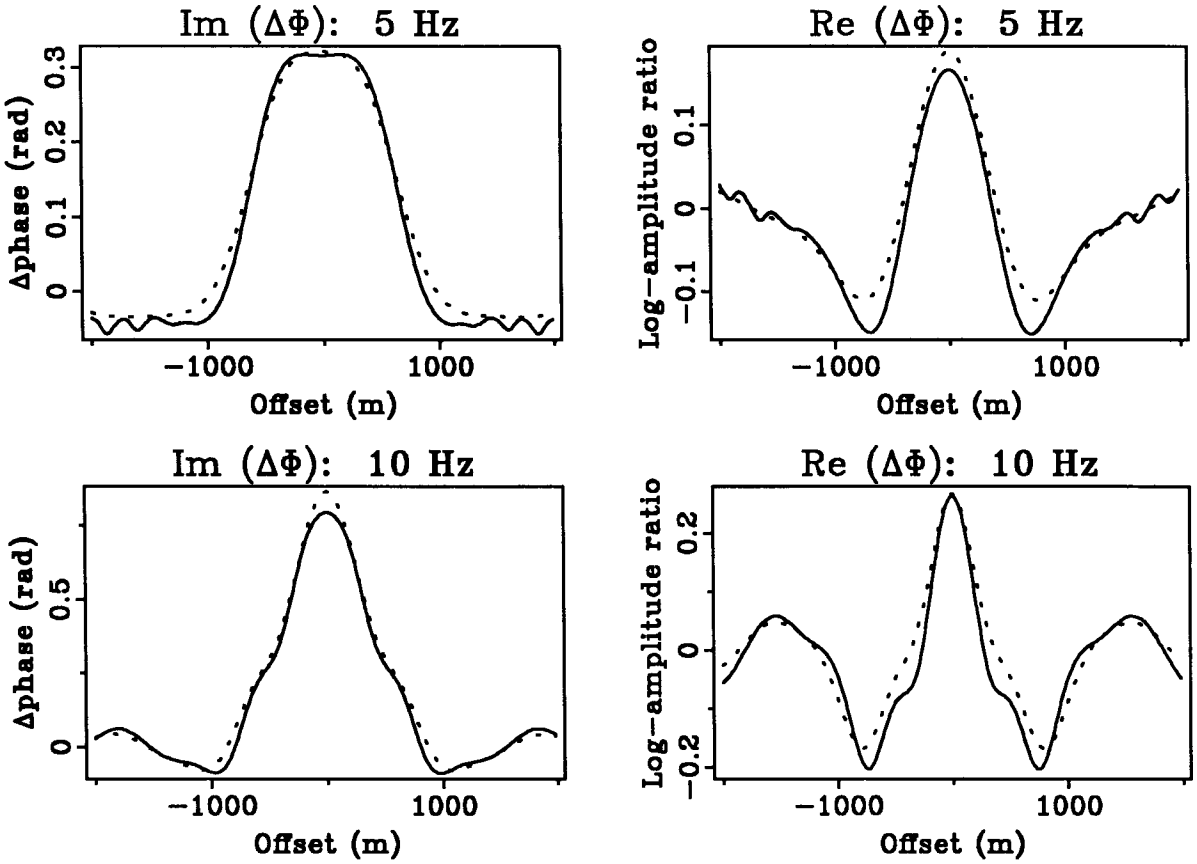

FIG. 11. Forward-modelled (dotted) and measured (solid) data for 5 and 10 Hz.

offset, they occur at that frequency for which the first Fresnel zone just encompasses the anomaly. When the anomaly protrudes into the second Fresnel zone, it underlies a negative portion of the wavepath, and contributes to a differential phase measurement of opposite sign. The 1060 m offset is particularly interesting in that it predicts a phase advance. For this offset, the anomaly is sensed more strongly by the second Fresnel zone (and negative part of the wavepath) than by the first.

Several relative maxima and minima in Figure 8 can be predicted by inspection of Figure 10. Here the boundaries of the first five Fresnel zones for several frequencies are shown superimposed on the circular velocity anomaly. The sign of each wavepath alternates from positive to negative, starting with a positive sign in the central zone. When the edge of the anomaly just grazes the inside boundary of a negative oscillation, it produces a relative minimum; when the edge grazes the inside boundary of a positive oscillation, it produces a relative maximum. The plots illustrate relative minima and maxima at 11 and 17 Hz for the 360 m offset trace, and at 8 and 11 Hz for the 1060 m offset trace.

Figure 11 compares forward-modelled data and measured data for 5 and 10 Hz. The solid lines show the real data, the dotted lines the modelled data. For this data set, full wave-equation modelling was well approximated by linearization of the wave-equation under the Rytov assumption.

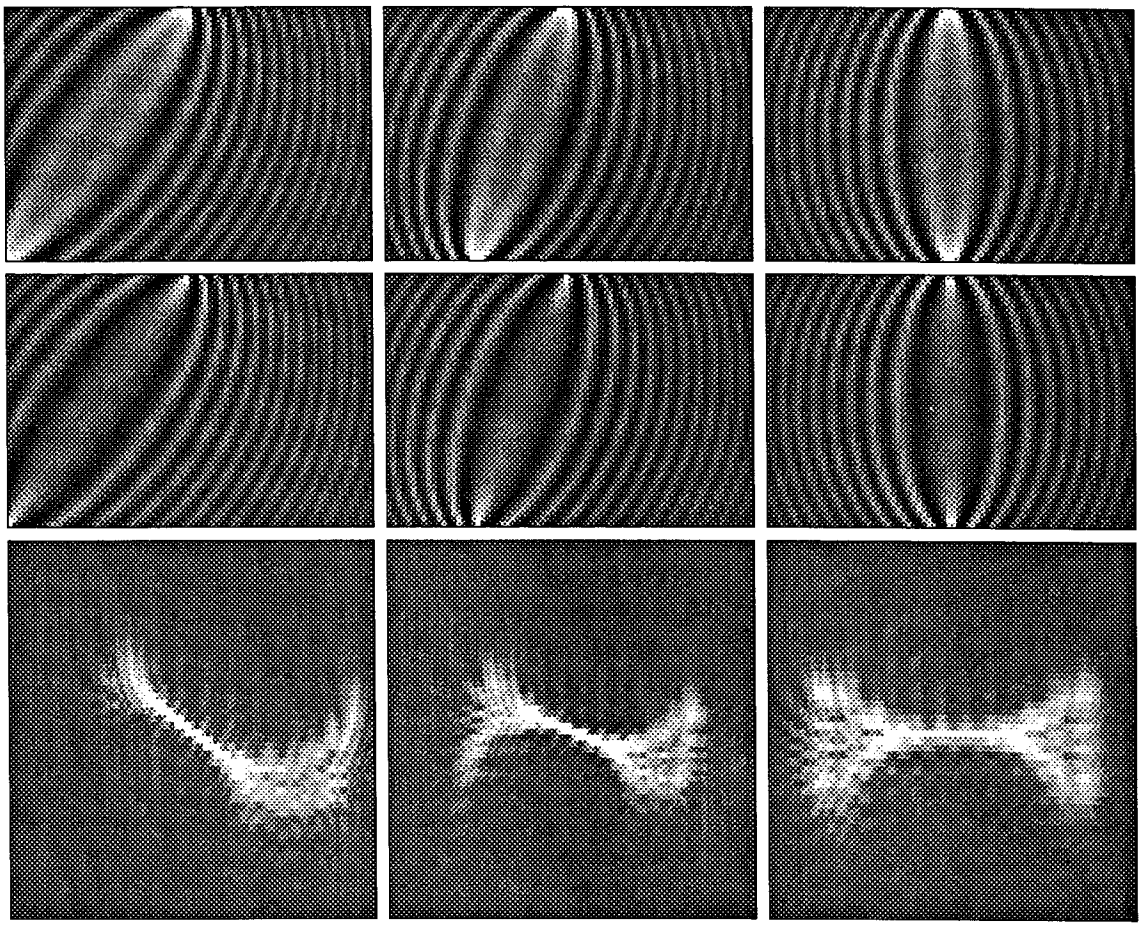

FIG. 12. The top two panels show the abbreviated imaginary and real parts of the 10 Hz monochromatic wavepath, for offsets of 1480, 760 and 0 m. The bottom panel shows the spatial-amplitude spectrum of each wavepath.

NUMERICAL EXAMPLE—INVERSION

This section inverts the data set described in the last section, solving the systems of equations $\mathcal{L}\Delta v/v = \Delta\phi$ and $L\Delta\omega = \Delta t$ for wave-equation and ray-theoretic tomography, respectively. The section is divided into two subsections. The first uses the method of singular-value decomposition to evaluate the number of degrees of freedom available in wave-equation tomography and ray-theoretic tomography. In addition to a comparison between the two methods, three questions are addressed: are differential phase and log-amplitude ratios independent; how finely should the data be sampled in space; how finely should the data be sampled in frequency. The second subsection compares ray-theoretic and wave-equation tomographic inversion results, as computed using the linear system solver LSQR (Paige and Saunders, 1982).

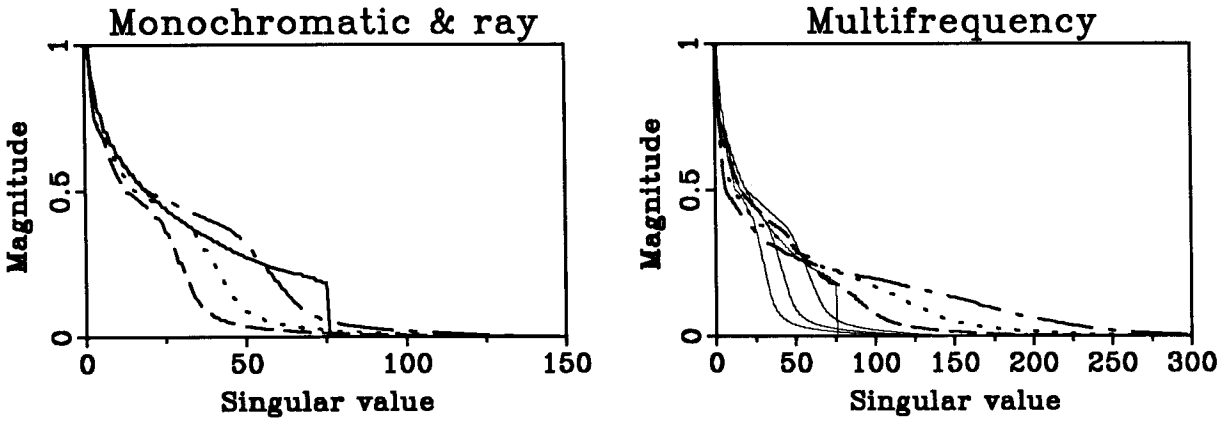

FIG. 13. (a) Singular values for ray-theoretic tomography (solid line) and monochromatic 5 (dashed), 7.5 (dotted) and 10 (dot-dashed) Hz wave-equation tomography. (b) Singular values of (a) overlain by singular values for multifrequency inversions: 5 and 10 Hz (dashed); 5, 7.5 and 10 Hz (dotted); 5, 6, 7, 8, 9, 10 Hz (dot-dashed).

Degrees of freedom analysis

For reasons of computational efficiency the experiment described above was subsampled. The geophone spacing was increased from 10 m to 40 m and the maximum offset was reduced from 2000 m to 1480 m. This subsampling translates to 3700 model parameters and 75 offsets. It also means that the wavepaths were truncated in space by the dimensions of the model space. The top part of Figure 12 shows the abbreviated 10 Hz wavepaths for three different offsets; the lower part of Figure 12 shows the spectra of the limited patterns, as they sweep over the (k_x, k_z) plane. Spectral coverage falls off at approximately $2\sqrt{2}k_0$ (Rocca and Woodward, 1988).

Figure 13 shows plots of singular values computed by an SVD program for different subsets of the data. Figure 13a compares ray-theoretic tomography to monochromatic, wave-equation tomography for three different frequencies (5, 7.5 and 10 Hz). Ray-theoretic tomography has 75 significant singular values, one for each offset (or equivalently, one for each equation). While each of the wave-equation tomographic inversions had 150 equations (2 equations for each offset), their number of significant singular values varies by frequency. 5, 7.5 and 10 Hz have from 30 to 60, 45 to 90 and 60 to 120 significant singular values, respectively. This translates to 4 to 8 degrees of freedom per wavelength, instead of the usual 2. In this case the extra degrees of freedom come both from the independence of the amplitude and phase measurements, and from the fact that the monochromatic wavepaths yield some coverage in the spatial-frequency domain up to twice the source wavenumber. While not shown here, subsampling in space and omitting either the phase or log-amplitude equations produced results supporting these conclusions.

Figure 13b addresses the question of how finely the data should be sampled in frequency. It reproduces the singular-value curves from Figure 13a as faint lines, overlain by singular-value curves for multifrequency inversions as darker lines. The multifrequency experiments were run for: 5 and 10 Hz (300 equations); 5, 7.5 and 10 Hz (450 equations); and 5, 6, 7, 8, 9, and 10 Hz (900 equations). There appears to be substantial independent information even when the data is sampled at 1 Hz. Since the wavepaths were sampled over 2000 m, the sampling rate in the wavenumber domain was .0005 cycles/m. Contemplation of the spatial-amplitude spectra in Figure 12 suggests that their boundaries change by more than .0005 cycles/m for a 1 Hz change in source frequency. As long as the sampling in frequency shifts these boundaries by more than the spatial-frequency resolution of the experiment, adding more frequencies will add more information.

Inversion

Figure 14 shows the result of applying LSQR to the data described in the previous section. The top two panels show the model and the ray-theoretic inversion. Since Figure 8 demonstrated that the assumptions of ray theory are not met by this data set, the ray-theoretic inversion was run with perfect, raytraced data. (The issue of dispersion and event picking has been discussed elsewhere by Wielandt, 1987.) The poor result arises from the large null space in the ray-theoretic problem: the ray interrogates a very limited region of the model. Many more shots would be required to fully illuminate the anomaly.

The second two panels show monochromatic, 5 Hz and 10 Hz wave-equation inversions, respectively. Clearly, wave-equation tomography makes much fuller use of the information in the seismic experiment than does ray-theoretic tomography. For unwindowed data, each shot-geophone experiment interrogates the full model space. Even though the monochromatic inversions showed fewer significant singular values than the ray-theoretic inversion in Figure 13, they have succeeded in distinguishing the anomaly from the source position. The lower frequency (5 Hz) inversion does the best job of positioning the anomaly; the higher frequency inversion is more similar to the ray-theoretic result.

The bottom panels show multifrequency, wave-equation tomographic inversions: 5 and 10 Hz on the left; 5, 10, 15, 20 and 25 Hz on the right. The last was run with a finer (20 m) sampling rate, and included offsets up to 1580 m. (There were 15800 model parameters. The problem was not run to convergence, but stopped after 350 iterations.) The multifrequency inversions provide fairly clear representations of the anomaly. The five-frequency inversion even shows some promise of removing the false anomaly at the source. The elongation of the inverted anomaly in the z-direction arises from the familiar finite-aperture, limited-cable-length problem of tomography. Without horizontally-placed shots and geophones, the spectral patterns of Figure 12 never sweep across the k_z axis.

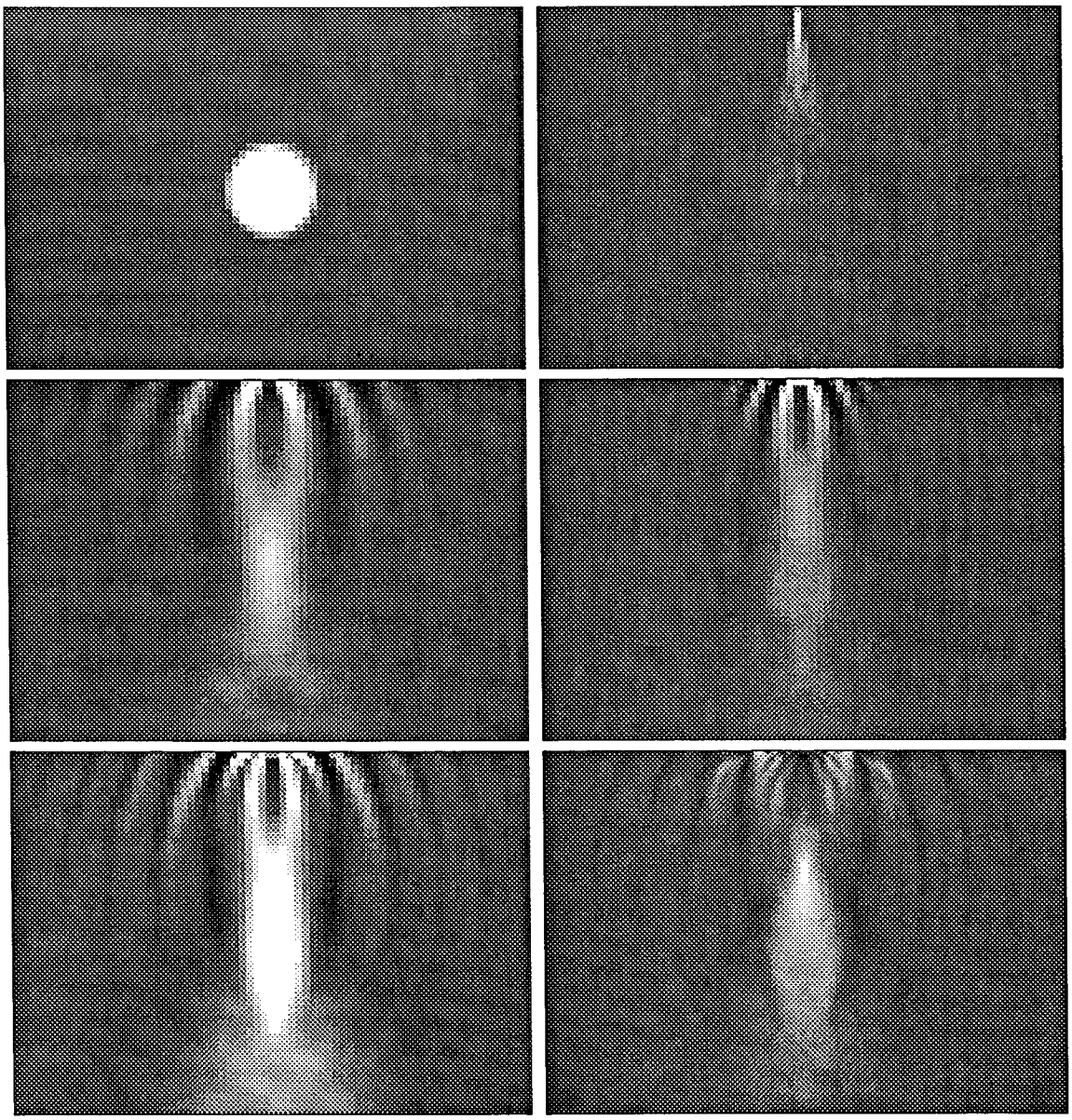

FIG. 14. Inversion results. From left to right, top to bottom: the model; a ray-theoretic inversion; a monochromatic 5 Hz wave-equation inversion; a monochromatic 10 Hz inversion; a multifrequency 5 and 10 Hz inversion; a multifrequency 5, 10, 15, 20 and 25 Hz inversion.

CONCLUSION

Ray and diffraction tomography make different assumptions about the availability of information in the seismic experiment. Working in the time domain, the first method assumes a nondispersive medium and a source of infinite bandwidth; for a single source-geophone experiment, it measures a single traveltime delay. Working in the temporal-frequency domain, the second method accommodates dispersive media but assumes event windows of infinite length; for a single source-geophone experiment, it measures phase delays and amplitude changes as a function of frequency.

As monochromatic *raypaths*, the *wavepaths* of space-domain, wave-equation tomography provide a link between ray and diffraction tomography. They furnish a conceptual tool for modifying the two methods when their respective assumptions are violated. When ray-theoretic tomography is applied to a bandlimited source in a nondispersive medium, wavepath analysis tells us to project traveltimes back over broad, bandlimited raypaths—formed by averaging wavepaths over the source bandwidth. When wave-theoretic tomography is applied to time-windowed data, similar analysis tells us to project differential phases and amplitudes back over smoothed wavepaths—formed by convolving monochromatic wavepaths with the Fourier transform of the time-domain window.

The wavepaths discussed in this paper were confined to constant background fields and cross-hole geometries. Their theory must be developed before they can describe more complicated media and the virtual sources of reflection tomography. For any application, their formulation in the space domain increases the flexibility of the wave-theoretic, tomographic method in dealing with irregularly sampled surveys of finite length.

ACKNOWLEDGMENTS

I wish to thank: Fabio Rocca for his enthusiasm, interest and innumerable consultations; John Etgen for both his advice and his finite-difference modelling program; and Paul Fowler and Jos van Trier, for many helpful discussions.

BIBLIOGRAPHY

Bleistein, N., 1984, Mathematical methods for wave phenomena: Academic Press, 18.

Devaney, A. J., 1982, A filtered backpropagation algorithm for diffraction tomography: Ultrasonic Imaging, **4**, 336–350.

Fawcett, J. A., and Clayton, R. W., 1984, Tomographic reconstruction of velocity anomalies: Bull. Seis. Soc. Am., **74**, 2201–2219.

Paige, C., and Saunders, M., 1982, LSQR: an algorithm for sparse linear equations and sparse least squares: ACM Trans. Math. Softw., **8**, 43–71.

Rocca, F., and Woodward, M. J., 1988, Wave-equation tomography–II: SEP–**57**.

Slaney, M., Kak, A. C., and Larsen, L., 1984, Limitations of imaging with first-order diffraction tomography: IEEE Trans. Microwave Theory and Techniques, MTT–**32**, 860–873.

Wielandt, E., 1987, On the validity of the ray approximation for interpreting delay times: Seismic Tomography, edited by G. Nolet, Riedel Publishing Company, 85–98.

Woodward, M. J., 1987, Reflection tomography: vees in midpoint-offset space: SEP–**51**, 1–12.

Woodward, M. J., 1986, Iterative tomography: error projection along ellipses and lines: SEP–**48**, 35–43.

Wu, R. S., and Toksoz, M. N., 1987, Diffraction tomography and multisource holography applied to seismic imaging: Geophysics, **52**, 11–25.

THE STANFORD UNIVERSITY
Campus Report

March 2, 1988

Claerbout, Macovski elected engineering academy members

Prof. Jon Claerbout of the Stanford School of Earth Sciences and Prof. Albert Macovski of the School of Engineering are among 85 scientists recently elected to membership in the National Academy of Engineering.

Claerbout, the Cecil and Ida Green professor of geophysics, was honored for "original and pioneering studies that revolutionized seismic wave analysis and greatly aided the international search for petroleum."

Macovski, professor of electrical engineering and radiology, was elected for "contributions to color television and to medical imaging, using computer processing and alternative illuminating sources."

Membership honors those who have made "important contributions to engineering theory and practice, including significant contributions to the literature of engineering," and those who have demonstrated "unusual accomplishment in new and developing fields of technology."